



<b>Publication Year</b>	2019
<b>Acceptance in OA</b>	2021-04-16T15:37:59Z
<b>Title</b>	Rotational and Rotational-Vibrational Raman Spectroscopy of Air to Characterize Astronomical Spectrographs
<b>Authors</b>	Vogt, Frédéric P. A., Kerber, Florian, Mehner, Andrea, Yu, Shanshan, Pfrommer, Thomas, Lo Curto, Gaspare, Figueira, Pedro, Parraguez, Diego, Pepe, Francesco A., Mégevand, Denis, RIVA, Marco, DI MARCANTONIO, Paolo, Lovis, Christophe, Amate, Manuel, MOLARO, Paolo, Cabral, Alexandre, Osorio, Maria Rosa Zapatero
<b>Publisher's version (DOI)</b>	10.1103/PhysRevLett.123.061101
<b>Handle</b>	<a href="http://hdl.handle.net/20.500.12386/30777">http://hdl.handle.net/20.500.12386/30777</a>
<b>Journal</b>	PHYSICAL REVIEW LETTERS
<b>Volume</b>	123

## Rotational and Rotational-Vibrational Raman Spectroscopy of Air to Characterize Astronomical Spectrographs

Frédéric P. A. Vogt,<sup>1,\*</sup> Florian Kerber,<sup>2</sup> Andrea Mehner,<sup>1</sup> Shanshan Yu,<sup>3</sup> Thomas Pfrommer,<sup>2</sup> Gaspare Lo Curto,<sup>1</sup> Pedro Figueira,<sup>1,4</sup> Diego Parraguez,<sup>1</sup> Francesco A. Pepe,<sup>5</sup> Denis Mégevand,<sup>5</sup> Marco Riva,<sup>6</sup> Paolo Di Marcantonio,<sup>7</sup> Christophe Lovis,<sup>5</sup> Manuel Amate,<sup>8</sup> Paolo Molaro,<sup>7</sup> Alexandre Cabral,<sup>9</sup> and Maria Rosa Zapatero Osorio<sup>10</sup>

<sup>1</sup>European Southern Observatory (ESO), Av. Alonso de Córdova 3107, 763 0355 Vitacura, Santiago, Chile

<sup>2</sup>European Southern Observatory (ESO), Karl-Schwarzschild-Str. 2, 85748 Garching, Germany

<sup>3</sup>Jet Propulsion Laboratory, California Institute of Technology, Pasadena, California, 91109, USA

<sup>4</sup>Instituto de Astrofísica e Ciências do Espaço, Universidade do Porto, CAUP, Rua das Estrelas, 4150-762 Porto, Portugal

<sup>5</sup>Observatoire Astronomique de l'Université de Genève, 51 chemin des Maillettes, 1290 Versoix, Switzerland

<sup>6</sup>Osservatorio Astronomico di Brera, INAF, Via Bianchi 46, 23807 Merate, Italy

<sup>7</sup>Osservatorio Astronomico di Trieste, INAF, Via Tiepolo 11, 34143 Trieste, Italy

<sup>8</sup>Instituto de Astrofísica de Canarias, C/ Vía Láctea, 38200 La Laguna, Tenerife, Spain

<sup>9</sup>Faculdade de Ciências, Instituto de Astrofísica e Ciências do Espaço, Universidade de Lisboa, Campo Grande, Edifício C8, 1749-016 Lisboa, Portugal

<sup>10</sup>Centro de Astrobiología (CSIC-INTA), Carretera de Ajalvir km 4, Torrejón de Ardoz, 28850 Madrid, Spain



(Received 15 April 2019; revised manuscript received 20 June 2019; published 6 August 2019)

Raman scattering enables unforeseen uses for the laser guide-star system of the Very Large Telescope. Here, we present the observation of one up-link sodium laser beam acquired with the ESPRESSO spectrograph at a resolution  $\lambda/\Delta\lambda \sim 140\,000$ . In 900 s on source, we detect the pure rotational Raman lines of  $^{16}\text{O}_2$ ,  $^{14}\text{N}_2$ , and  $^{14}\text{N}^{15}\text{N}$  (tentatively) up to rotational quantum numbers  $J$  of 27, 24, and 9, respectively. We detect the  $^{16}\text{O}_2$  fine-structure lines induced by the interaction of the electronic spin  $\mathbf{S}$  and end-over-end rotational angular momentum  $\mathbf{N}$  in the electronic ground state of this molecule up to  $N = 9$ . The same spectrum also reveals the  $\nu_{1\leftarrow 0}$  rotational-vibrational Q-branch for  $^{16}\text{O}_2$  and  $^{14}\text{N}_2$ . These observations demonstrate the potential of using laser guide-star systems as accurate calibration sources for characterizing new astronomical spectrographs.

DOI: [10.1103/PhysRevLett.123.061101](https://doi.org/10.1103/PhysRevLett.123.061101)

**Introduction.**—The 4 Laser Guide Star Facility [4LGSF; [1]] has been in operation on Unit Telescope 4 (UT4) of the Very Large Telescope (VLT) in Chile's Atacama desert since mid-2016. It is comprised of four 22 W continuous wave lasers, and forms an integral part of UT4's Adaptive Optics Facility [AOF; [2]]. Its lasers are used to excite sodium atoms in the mesosphere, primarily located in a layer several kilometers thick at an altitude of  $\sim 90$  km [3–5]. The four lasers each emit 18 W at 5891.59120 Å to excite the  $D_2a$  sodium transition, 2 W at 5891.571 37 Å to repump (via the  $D_2b$  line) sodium atoms “lost” to the  $3^2S_{1/2}F = 1$  state [with  $F$  the total atomic angular momentum quantum number; see [6]], and 2 W at 5891.611 03 Å that are not usable for adaptive optics (AO) purposes. The spectral stability of the lasers, of the order of  $\pm 3$  MHz  $\equiv 3.5$  fm over hours, is achieved by using a solid-state high-resolution wavelength meter. The absolute accuracy of the lasers ( $< 10$  MHz  $\equiv 11.6$  fm at the  $3\sigma$  level) is achieved via periodic calibrations of the wavelength meter against a stabilized Helium-Neon reference laser [7–9]. The resulting four wave front reference sources created in the mesosphere are exploited by the AO modules GALACSI [10,11] and

GRAAL [12] that are coupled to the astronomical instruments MUSE [13] and HAWK-I [14,15], respectively.

The 4LGSF was designed to work in concert with the other components of the AOF to enhance the image quality achieved by instruments on UT4. The MUSE observations of the inelastic Raman scattering of laser photons by air molecules above UT4 [16] have, however, opened unforeseen avenues for experimentation with the 4LGSF system in a *stand-alone* mode (by *stand-alone*, we mean that the 4LGSF is operated on its own, as opposed to the *nominal* mode in which the 4LGSF is slaved to the other components of the AOF to support AO observations with MUSE and HAWK-I). For example, telescope and instrument operators can easily vary the size of the square asterism of laser guide stars by using the laser pointing camera [17], without the need to interact with any of the other AOF components or UT4 instruments. This capability was used to monitor the flux of laser lines present in MUSE AO observations over a 27-month period, which revealed dust particles on the primary and tertiary telescope mirrors to be an important secondary scattering source for the laser photons [18]. Here, we discuss another stand-alone use

case for the 4LGSF, and laser guide-star systems in general: that of an accurate wavelength calibration source for astronomical spectrographs.

The Echelle SPectrograph for Rocky Exoplanets and Stable Spectroscopic Observations (ESPRESSO [19,20]) is an ultrastable fiber-fed high-resolution spectrograph installed in the Coudé facility of the VLT. The instrument delivers a spectral resolution  $\lambda/\Delta\lambda$  of  $\sim 140\,000$  (single UT, “HR” mode),  $\sim 190\,000$  (single UT, “UHR” mode), or  $\sim 70\,000$  (four UTs, “MR” mode). The spectrograph itself is temperature stabilized at the mK level in a  $10^{-5}$  hPa vacuum. Astronomical observations can be wavelength calibrated with a Th-Ar hollow-cathode lamp (which can be aided by a white-light Fabry-Pérot), or a dedicated laser frequency comb [21]. In particular, the existence of two parallel fibers allows to acquire scientific observations (in fiber “A”) with a simultaneous wavelength calibration exposure (in fiber “B”) to track internal radial velocity drifts over time. The overall instrument design is driven by the goal *precision* of  $10\text{ cm s}^{-1}$  over 10 years for radial-velocity measurements in a single UT mode. The goal wavelength *accuracy* of ESPRESSO, on the other hand, is  $10\text{ m s}^{-1}$ .

As with all new systems at the VLT, ESPRESSO underwent a series of commissioning observations to characterize its performances as built, following its installation at the Coudé focus, and prior to being offered to the general community. Characterizing the wavelength calibration accuracy of the spectrograph is evidently one of the high-priority goals for this activity. Ideally, this should be achieved by means of external reference sources that fully mimic real observations, and allows one to characterize the entire *telescope(s)*, *Coudé train*, and *instrument* assembly. The 4LGSF, and the associated Raman scattering of its laser photons by air molecules, provides the ideal means to do so. In this Letter, we present the first ESPRESSO observation of one 4LGSF up-link laser beam acquired during the commissioning phase of the instrument. Throughout the text, all quoted wavelengths are in vacuum.

*Observations and data reduction.*—The ESPRESSO spectrum presented in this Letter was acquired during commissioning activities on the night of February 2, 2018. The observations were performed from UT4, with the 4LGSF system operated in stand-alone mode, in parallel to ESPRESSO, which was entirely oblivious to it. The telescope was preset to place the ESPRESSO fiber A on an empty sky field, with no entries in the USNO-B1 catalog [which is complete down to  $V = 21$  mag; [22]]. Upon the end of the acquisition sequence, one 22 W laser guide-star was placed manually in the center of the VLT field of view using the laser pointing camera (LPC; see Fig. 1). Manual offsets were then applied to the jitter-loop mirror of the laser launch telescope to bring the up-link beam—clearly visible in the ESPRESSO Technical CCD of Front-End 4 for Field Acquisition [23]—into the field of

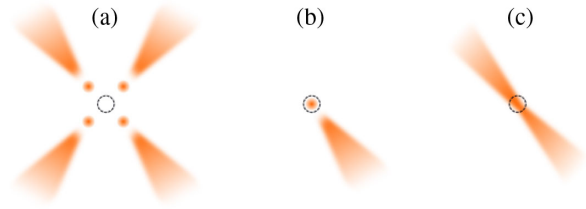


FIG. 1. Diagram (not to scale) of the manual acquisition steps for the ESPRESSO observations described in this article. (a) All 4LGSF lasers are propagating. The four laser guide-stars (orange dots) are positioned to a nominal square asterism using the LPC. From the instrument perspective, the up-link laser beams (visible up to  $\sim 35$  km of altitude) are located on the outside of the laser guide stars (located at  $\sim 90$  km of altitude). (b) Using the LPC, a single laser guide star is placed in centerfield. The propagation is stopped for all other laser guide stars. (c) The up-link beam is brought over the ESPRESSO fiber (black circle) using manual offsets applied to the jitter-loop mirror of the laser launch telescope. The focus of the telescope is adjusted to bring the beam better into focus at the location of the fiber.

view of the ESPRESSO fiber. The propagation of the other three laser guide-stars was stopped. The spectrum presented here corresponds to a single 900 s exposure, acquired in the HR21 mode ( $\lambda/\Delta\lambda \sim 140\,000$ ,  $1''$  fiber diameter on sky,  $2 \times 1$  pixel binning along the “spatial” direction). The observation was performed at an airmass of 1.01 (equivalent to a telescope altitude of  $81.7$  deg at the start), with 16 mm of precipitable water vapor (which is a very high value for Cerro Paranal which has a median of  $\sim 2.4$  mm [24,25]), a relative ambient humidity of 38%, an ambient pressure of 742.4 hPa, and a ground temperature of  $13.5^\circ\text{C}$ . The exact beam altitude probed is formally unknown: from our experience with MUSE (see the Appendix in Ref. [16]), we estimate it to be  $15 \pm 8$  km above ground. Given the perspective and the continuous-wave nature of the 4LGSF lasers, one has to note that a range of several kilometers is being sampled by the ESPRESSO fiber. Since the laser beam was not located at infinity, the secondary mirror of UT4 was offset by  $+4$  mm to bring the beam into better focus, and thus increase the observed beam surface brightness.

The data were reduced using the ESPRESSO pipeline v1.1.4. The wavelength calibration was derived from reference exposures (in fiber A) obtained with the laser frequency comb during the daily instrument calibrations.

*Results.*—We present in Figs. 2 and 3 a subset of the ESPRESSO spectrum of one up-link laser beam from the 4LGSF. Figure 2 contains an overall view of the pure rotational Raman lines and the  $\nu_{1\leftarrow 0}$  rotational-vibrational (ro-vibrational) Raman lines for  $^{16}\text{O}_2$  and  $^{14}\text{N}_2$ , readily visible as a resolved forest of lines. In Fig. 3, we present a detailed view of the spectral regions located within  $\pm 70$  Å from the main laser line. To identify the specific origin of each line in the spectrum, we first compare it with the analytical predictions of the rotational and ro-vibrational

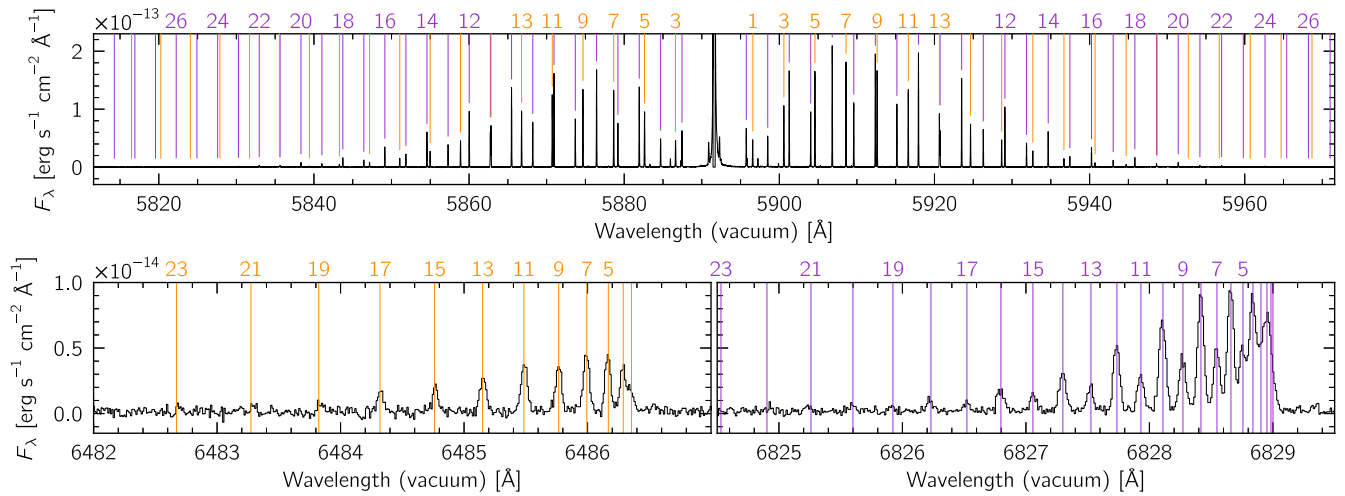


FIG. 2. ESPRESSO view of the pure rotational Raman lines (top), and  $Q$  branch of the ro-vibrational Raman lines of  $^{16}\text{O}_2$  (bottom left) and  $^{14}\text{N}_2$  (bottom right), associated with one 4LGSF up-link laser beam. Orange (for  $^{16}\text{O}_2$ ) and purple (for  $^{14}\text{N}_2$ ) lines mark the theoretical position of each Raman line derived with the model of nonrigid singlet diatomic rotators (see the Supplemental Material [31] for details). Colored integers denote the rotational quantum number  $J$  associated with the different analytical wavelength predictions. The CCD did saturate within  $\pm 0.2 \text{ \AA}$  of the main laser line.

Raman lines for homonuclear diatomic molecules treated as nonrigid singlet rotators (see the Supplemental Material SM for the full analytical derivation, which includes Refs. [26–30]). We unambiguously detect pure rotational lines up to a molecular rotational quantum number  $J = 27$  for  $^{16}\text{O}_2$  and  $J = 24$  for  $^{14}\text{N}_2$ . The lines in the  $\nu_{1\leftarrow 0}$  ro-vibrational  $Q$  branch of  $^{14}\text{N}_2$  and  $^{16}\text{O}_2$  are resolved from  $J \gtrsim 4$ , and unambiguously detected up to  $J \sim 18$ . For  $^{16}\text{O}_2$ , only lines associated with odd values of  $J$  are detected, as expected from the selection rules imposed by quantum mechanics for homonuclear diatomic molecules with zero nuclear spin [26].

We also detect the pure rotational Raman lines from  $^{14}\text{N}^{15}\text{N}$  (tentatively) up to  $J = 9$ . These lines are detected with a signal-to-noise ratio  $\cong 2 \pm 1$ : insufficient to formally rule out  $^{14}\text{N}_2^+$  as the molecule responsible, from the theoretical line wavelengths alone (see the Supplemental Material [31] for details). To try to discriminate between  $^{14}\text{N}^{15}\text{N}$  and  $^{14}\text{N}_2^+$ , we assembled a simple model of two Gaussian lines with their dispersion tied, to individually fit each of the tentative  $^{14}\text{N}^{15}\text{N}$  lines alongside the nearest  $^{14}\text{N}_2$  line (i.e., associated to the same  $J$  value). From a Markov-Chain Monte Carlo sampling of the individual posterior distribution of each of the clearest 14 line pairs, assuming a least-square likelihood and flat priors with a lower bound of 0 for the line intensities and dispersion, we find no evidence for an alternating intensity pattern between lines associated with even and odd  $J$  values, as one would expect from  $^{14}\text{N}^+$ . On the other hand, we derive an overall line intensity ratio of  $0.5_{-0.3}^{+0.6}\%$  (68% confidence level) with respect to the nearest  $^{14}\text{N}_2$  lines, consistent with the atmospheric abundance ratio of  $^{14}\text{N}^{15}\text{N}$  to  $^{14}\text{N}_2$  [32].

Clearly, deeper observations are necessary to confirm this identification.

Altogether, the analytical predictions account for most of the rotational and all of the ro-vibrational lines visible in the ESPRESSO spectrum, but fail to explain a series of fainter lines in the vicinity of the main laser line. We link the majority of these fainter lines to the existence of a nonzero electronic spin in the ground state  $^3\Sigma_g^-$  of  $^{16}\text{O}_2$ . It is the interaction between this electronic spin and the molecular rotation that leads to the fine splitting of the pure rotational Raman lines of  $^{16}\text{O}_2$ . From an exhaustive numerical modeling of this effect (see the Supplemental Material SM for details, which includes Refs. [33–36]), we can successfully identify side-lines up to  $N = 9$  (where  $N$  denotes the end-over-end rotation). We are left with six lines of (yet) unknown origin, all located within  $13 \text{ \AA}$  from the main laser line (see Fig. 3).

*Discussion.*—Up until now, the majority of observations of the up-link beams from laser guide-star systems at astronomical observatories would have resulted from the unintentional *collision* between neighboring telescopes: an observational nuisance against which dedicated coordination tools were promptly developed [37–40]. The fact remains, however, that propagating a laser beam through the atmosphere entails a range of physical phenomena, some of which are unrelated to the creation of artificial reference wave front sources in support of AO systems. Raman scattering, in particular, implies that initially monochromatic up-link laser beams possess a rich spectral signature, with numerous lines located several tens (for pure rotational Raman lines) up to several hundreds (for ro-vibrational Raman lines) of  $\text{\AA}$  away from the main laser line. This may

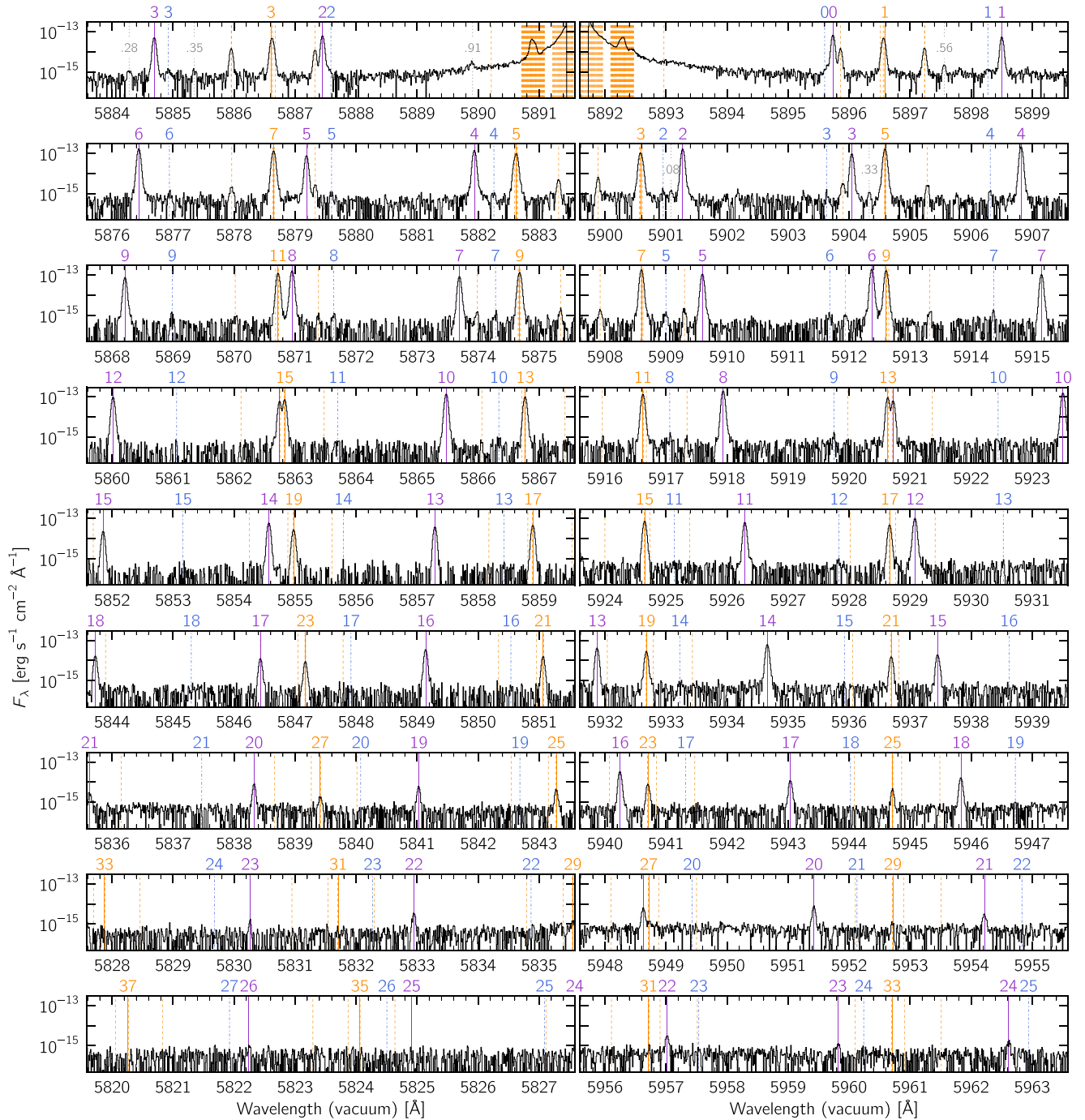


FIG. 3. ESPRESSO spectrum of one 4LGSF up-link laser beam, focusing on the spectral regions containing pure rotational Raman lines. Each panel is 8 Å wide. For a given row, the left and right panels are equidistant from the main laser line at 5891.5912 Å (which is saturated). Pure rotational Raman lines, associated with the Stokes (right column) and anti-Stokes (left column) branches, are detected up to  $J = 27$  for  $^{16}\text{O}_2$ ,  $J = 24$  for  $^{14}\text{N}_2$ , and  $J = 9$  for  $^{14}\text{N}^{15}\text{N}$ . Solid orange, solid purple, and dash-dotted blue vertical lines mark the theoretical position of the pure rotational Raman lines of  $^{16}\text{O}_2$ ,  $^{14}\text{N}_2$ , and  $^{14}\text{N}^{15}\text{N}$  (respectively), when treated as nonrigid singlet diatomic rotators. The molecular rotational quantum number  $J$  associated with each of these lines is indicated above them (only the  $^{14}\text{N}_2$   $J = 11$  anti-Stokes and  $J = 9, 19$  Stokes lines are not tagged because of crowding). Dashed orange vertical lines, derived using a numerical model of  $^{16}\text{O}_2$  accounting for the nonzero electronic spin of its ground state, highlight the fine-splitting of the pure rotational lines for this molecule. The nature of six lines (tagged with dotted grey vertical lines and the first two decimals of their wavelength in the top panels) remains unknown at this time.

drive specific design choices for the next generation of optical AO instruments relying on laser guide-star systems. Under specific circumstances, for example with an on-axis laser guide-star system, pure rotational Raman lines more than one order of magnitude brighter than sky lines may potentially be found  $\geq 50$  Å away from the main laser line, as illustrated in Fig. 2. This might require the use of notch filters with a specific spectral width, should a cost-benefit analysis [balancing the scientific benefit(s) of increased wavelength coverage with the spectral contamination of rotational Raman lines] warrant it.

The inelastic Raman scattering of laser photons provides an ideal means to characterize the new ESPRESSO spectrograph at the VLT, and validate the wavelength solution of its data product over a spectral range of  $\sim 1000$  Å. The possible presence of wind along the line of sight (and thus the spectral shifting of the signal over time) implies that the Raman lines are not suitable to characterize the goal *precision* of  $10 \text{ cm s}^{-1}$  over 10 years for radial velocity measurements with ESPRESSO. We find, however, that the accuracy with which the Raman lines ( $< 5$  fm for the case of  $^{16}\text{O}_2$ ; see the Supplemental Material [31] for details) and the exciting laser wavelength ( $< 11.6$  fm at the  $3\sigma$  level) are known is ideally matched to the target *accuracy* of ESPRESSO of  $10 \text{ m s}^{-1} \equiv 20$  fm at the 4LGSF laser wavelength. The 4LGSF lasers have a spectral full width at half maximum  $\lesssim 5$  MHz  $\equiv 6$  fm, so that the full width at half maximum of the observed Raman lines is actually dominated by thermal broadening (of the order of 2.3 GHz for  $^{14}\text{N}_2$  and 2.1 GHz for  $^{16}\text{O}_2$  at 273 K). We find that measuring line-centroid values with an accuracy  $< 10$  fm requires peak-to-noise values larger than  $\sim 200$ . This was achieved, for the pure-rotational Raman lines of  $^{14}\text{N}_2$  and  $^{16}\text{O}_2$  in the ESPRESSO spectrum presented in Fig. 3, up to  $J \sim 15$  for both molecules.

The presence of wind shifts along the line of sight during such an observation can be easily minimized by pointing the telescope, on a quiet night, at a low airmass and at 90 deg from the dominant wind direction at high altitude. Doing so will restrict the spectral offsets caused by wind shifts to those associated with vertical motions, which can be expected to be less than  $1 \text{ m s}^{-1} \equiv 2$  fm [41]. We voluntarily do not present here the formal characterization of the spectral accuracy of ESPRESSO. It will be discussed by the instrument Consortium in a separate publication, together with the required modeling of the instrument line spread function that falls outside of the scope of this Letter.

The growing number of laser guide-star systems in operation [42] implies that the physics of Raman scattering is readily accessible to many professional astronomical telescopes worldwide: either directly, or via voluntary laser *collisions* with neighboring facilities (at sites hosting multiple observatories). As the power of new generations of laser guide-star systems increases, so does the flux of the associated Raman lines, which reduces the amount of time

required to acquire spectra with sufficient signal to noise for an accurate instrumental characterization. The molecular physics potentially accessible via Raman scattering is undeniably very rich, as evidenced by its extensive use for atmospheric studies [43–52]. For astronomers, the  $^{14}\text{N}_2$  and  $^{16}\text{O}_2$  molecules are undoubtedly the best molecules to focus on. As the prime constituents of Earth’s atmosphere, these homonuclear diatomic molecules will provide the strongest Raman signal, which is nowadays very well characterized. In essence, our ESPRESSO observation of one 4LGSF up-link laser beam paints the picture of a future in which laser guide-star systems at astronomical observatories will not only be thought of as mere subcomponents of complex adaptive optics systems, but also as bright, flexible, and accurate calibration sources for characterizing new generations of astronomical spectrographs.

We thank Ronald Holzlöhner for enlightening conversations, Jorge Lillo-Box and Álvaro Ribas for sharing their expertise in MCMC techniques with us, Susana Cerda and Rodrigo Romero for their operational support during part of the ESPRESSO commissioning run, and the AOF Builders [2] for the construction and installation of the AOF on UT4 at the VLT. We are very grateful to the ESO librarians for the outstanding support of our bibliographic excursions beyond the astrophysical realm. This research has made use of the following PYTHON packages: MATPLOTLIB [53], ASTROPY, a community-developed core PYTHON package for Astronomy [54,55], APLPY, an open-source plotting package for PYTHON [56], FCMAKER [57,58], a PYTHON module to create ESO-compliant finding charts for OBs on *p2*, ASTROQUERY [59], which provides a set of tools for querying astronomical web forms and databases [60], ASTROPLAN [61], and EMCEE [62]. This research has also made use of the ALADIN interactive sky atlas [63], of SAOIMAGE DS9 [64] developed by Smithsonian Astrophysical Observatory, and of NASA’s Astrophysics Data System. Portions of this Letter present research carried out at the Jet Propulsion Laboratory, California Institute of Technology, under contract with the National Aeronautics and Space Administration. Government sponsorship is acknowledged. The Portuguese contribution to this work was supported by the Science and Technology Foundation FCT/MCTES through national funds and by FEDER - Fundo Europeu de Desenvolvimento Regional through COMPETE2020 - Programa Operacional Competitividade e Internacionalização through Grants No: UID/FIS/04434/2019; PTDC/FIS-AST/32113/2017 & POCI-01-0145-FEDER-032113; PTDC/FIS-AST/28953/2017 & POCI-01-0145-FEDER-028953; PTDC/FIS-AST/29245/2017; PTDC/FIS-AST/1526/2014. Based on observations made with ESO Telescopes at the La Silla Paranal Observatory under Program ID 60.A-9128(C). All the observations described in this article are freely available online from the ESO Data Archive. F. P. A. V. acknowledges an ESO Fellowship.

- \*frederic.vogt@alumni.anu.edu.au
- [1] D. Bonaccini Calia, W. Hackenberg, R. Holzlöhner, S. Lewis, and T. Pfrommer, The four-laser guide star facility: Design considerations and system implementation, *Adv. Opt. Technol.* **3**, 345 (2014).
- [2] R. Arsenault, P.-Y. Madec, J. Paufigue, P. La Penna, S. Stroebele, E. Vernet, J.-F. Pirard, W. Hackenberg, H. Kuntschner, J. Kolb *et al.*, The ESO adaptive optics facility under test, in *Proceedings of the Third AO4ELT Conference* (2013), p. 118.
- [3] N. Moussaoui, B. R. Clemesha, R. Holzlöhner, D. M. Simonich, D. Bonaccini Calia, W. Hackenberg, and P. P. Batista, Statistics of the sodium layer parameters at low geographic latitude and its impact on adaptive-optics sodium laser guide star characteristics, *Astron. Astrophys.* **511**, A31 (2010).
- [4] B. Neichel, C. D’Orgeville, J. Callingham, F. Rigaut, C. Winge, and G. Trancho, Characterization of the sodium layer at Cerro Pachón, and impact on laser guide star performance, *Mon. Not. R. Astron. Soc.* **429**, 3522 (2013).
- [5] T. Pfrommer and P. Hickson, High resolution mesospheric sodium properties for adaptive optics applications, *Astron. Astrophys.* **565**, A102 (2014).
- [6] R. Holzlöhner, S. M. Rochester, D. Bonaccini Calia, D. Budker, J. M. Higbie, and W. Hackenberg, Optimization of cw sodium laser guide star efficiency, *Astron. Astrophys.* **510**, A20 (2010).
- [7] A. Friedenauer, V. Karpov, D. Wei, M. Hager, B. Ernstberger, W. R. L. Clements, and W. G. Kaenders, RFA-based 589-nm guide star lasers for ESO VLT: A paradigm shift in performance, operational simplicity, reliability, and maintenance, *Proc SPIE* **8447**, 84470F (2012).
- [8] M. Enderlein, A. Friedenauer, R. Schwerdt, P. Rehme, D. Wei, V. Karpov, B. Ernstberger, P. Leisching, W. R. L. Clements, and W. G. Kaenders, Series production of next-generation guide-star lasers at TOPTICA and MPBC, *Proc SPIE* **9148**, 914807 (2014).
- [9] S. Lewis, D. B. Calia, B. Buzzoni, P. Duhoux, G. Fischer, I. Guidolin, A. Haimerl, W. Hackenberg, R. Hinterschuster, R. Holzlöhner *et al.*, Laser guide star facility upgrade, *The Messenger* **155**, 6 (2014).
- [10] R. Stuik, R. Bacon, R. Conzelmann, B. Delabre, E. Fedrigo, N. Hubin, M. Le Louarn, and S. Ströbele, GALACSI—The ground layer adaptive optics system for MUSE, *New Astron. Rev.* **49**, 618 (2006).
- [11] P. La Penna, E. Aller Carpentier, J. Argomedo, R. Arsenault, R. D. Conzelmann, B. Delabre, R. Donaldson, F. Gago, P. Gutierrez-Cheetam, N. Hubin *et al.*, AOF: Standalone test results of GALACSI, *Proc SPIE* **9909**, 99092Z (2016).
- [12] J. Paufigue, A. Bruton, A. Glindemann, A. Jost, J. Kolb, L. Jochum, M. Le Louarn, M. Kiekebusch, N. Hubin, P.-Y. Madec *et al.*, GRAAL: A seeing enhancer for the NIR wide-field imager Hawk-I, *Proc SPIE* **7736**, 77361P (2010).
- [13] R. Bacon, M. Accardo, L. Adjali, H. Anwand, S. Bauer, I. Biswas, J. Blaizot, D. Boudon, S. Brau-Nogue, J. Brinchmann *et al.*, The MUSE second-generation VLT instrument, *Proc SPIE* **7735**, 773508 (2010).
- [14] M. Kissler-Patig, J.-F. Pirard, M. Casali, A. Moorwood, N. Ageorges, C. Alves de Oliveira, P. Baksai, L. R. Bedin, E. Bendek, P. Biereichel *et al.*, HAWK-I: The high-acuity wide-field K-band imager for the ESO Very Large Telescope, *Astron. Astrophys.* **491**, 941 (2008).
- [15] R. Siebenmorgen, G. Carraro, E. Valenti, M. Petr-Gotzens, G. Brammer, E. Garcia, and M. Casali, The science impact of HAWK-I, *The Messenger* **144**, 9 (2011).
- [16] F. P. A. Vogt, D. Bonaccini Calia, W. Hackenberg, C. Opitom, M. Comin, L. Schmidtobreik, J. Smoker, I. Blanchard, M. Espinoza Contreras, I. Aranda *et al.*, Detection and Implications of Laser-Induced Raman Scattering at Astronomical Observatories, *Phys. Rev. X* **7**, 021044 (2017).
- [17] D. Bonaccini Calia, M. Centrone, F. Pedichini, A. Ricciardi, A. Cerruto, and F. Ambrosino, Laser guide star pointing camera for ESO LGS Facilities, *Proc SPIE* **9148**, 91483P (2014).
- [18] F. P. A. Vogt, J. Luis Álvarez, D. Bonaccini Calia, W. Hackenberg, P. Bourget, I. Aranda, C. Bellhouse, I. Blanchard, S. Cerda, C. Cid *et al.*, Raman-scattered laser guide-star photons to monitor the scatter of astronomical telescope mirrors, *Astron. Astrophys.* **618**, L7 (2018).
- [19] F. A. Pepe, S. Cristiani, R. Rebolo Lopez, N. C. Santos, A. Amorim, G. Avila, W. Benz, P. Bonifacio, A. Cabral, P. Carvas *et al.*, ESPRESSO: The Echelle spectrograph for rocky exoplanets and stable spectroscopic observations, *Proc SPIE* **7735**, 77350F (2010).
- [20] F. Pepe, S. Cristiani, R. Rebolo, N. C. Santos, H. Dekker, D. Mégevand, F. M. Zerbi, A. Cabral, P. Molaro, P. Di Marcantonio *et al.*, ESPRESSO—An Echelle Spectrograph for Rocky Exoplanets Search and Stable Spectroscopic Observations, *The Messenger* **153**, 6 (2013).
- [21] G. Lo Curto, L. Pasquini, A. Manescau, R. Holzwarth, T. Steinmetz, T. Wilken, R. Probst, T. Udem, T. W. Hänsch, J. González Hernández *et al.*, Astronomical spectrograph calibration at the exo-Earth detection limit, *The Messenger* **149**, 2 (2012).
- [22] D. G. Monet, S. E. Levine, B. Canzian, H. D. Ables, A. R. Bird, C. C. Dahn, H. H. Guetter, H. C. Harris, A. A. Henden, S. K. Leggett *et al.*, The USNO-B catalog, *Astron. J.* **125**, 984 (2003).
- [23] P. Duhoux, J. Knudstrup, P. Lilley, P. Di Marcantonio, R. Ciriame, and M. Mannelta, VLT instruments: Industrial solutions for non-scientific detector systems, *Proc SPIE* **9152**, 91520I (2014).
- [24] F. Kerber, T. Rose, A. Chacón, O. Cuevas, H. Czekala, R. Hanuschik, Y. Momany, J. Navarrete, R. R. Querel, A. Smette *et al.*, A water vapour monitor at Paranal observatory, *Proc SPIE* **8446**, 84463N (2012).
- [25] F. Kerber, R. R. Querel, R. Rondanelli, R. Hanuschik, M. van den Ancker, O. Cuevas, A. Smette, J. Smoker, T. Rose, and H. Czekala, An episode of extremely low precipitable water vapour over Paranal observatory, *Mon. Not. R. Astron. Soc.* **439**, 247 (2014).
- [26] G. Herzberg, *Molecular Spectra and Molecular Structure. Vol. 1: Spectra of Diatomic Molecules*, 2nd ed. (Van Nostrand Reinhold, New York, 1950).
- [27] M. Shimauchi, T. Miura, and H. Takuma, Determination of molecular constants of the X3Σg-state of O<sub>2</sub>, *Jpn. J. Appl. Phys.* **34**, L1689 (1995).
- [28] M. L. Orlov, J. F. Ogilvie, and J. W. Nibler, High-resolution coherent Raman spectra of vibrationally excited 14N<sub>2</sub> and 15N<sub>2</sub>, *J. Mol. Spectrosc.* **185**, 128 (1997).

- [29] J. Bendtsen, High-resolution Fourier transform Raman spectra of the fundamental bands of  $^{14}\text{N}^{15}\text{N}$  and  $^{15}\text{N}_2$ , *J. Raman Spectrosc.* **32**, 989 (2001).
- [30] K.-P. Huber and G. Herzberg, *Molecular Spectra and Molecular Structure. Vol. 4: Constants of Diatomic Molecules* (Van Nostrand Reinhold, New York, 1979).
- [31] See the Supplemental Material at <http://link.aps.org/supplemental/10.1103/PhysRevLett.123.061101> for the full derivation of the relevant Raman line wavelengths.
- [32] G. Junk and H. J. Svec, The absolute abundance of the nitrogen isotopes in the atmosphere and compressed gas from various sources, *Geochim. Cosmochim. Acta* **14**, 234 (1958).
- [33] S. Yu, B. J. Drouin, and C. E. Miller, High resolution spectral analysis of oxygen. IV. Energy levels, partition sums, band constants, RKR potentials, Franck-Condon factors involving the  $X^3\Sigma_g^-$ ,  $a^1\Delta_g$  and  $b^1\Sigma_g^+$  states, *J. Chem. Phys.* **141**, 174302 (2014).
- [34] S. Yu, C. E. Miller, B. J. Drouin, and H. S. P. Müller, High resolution spectral analysis of oxygen. I. Isotopically invariant Dunham fit for the  $X^3\Sigma_g^-$ ,  $a^1\Delta_g$ ,  $b^1\Sigma_g^+$  states, *J. Chem. Phys.* **137**, 024304 (2012).
- [35] B. J. Drouin, H. Gupta, S. Yu, C. E. Miller, and H. S. P. Müller, High resolution spectral analysis of oxygen. II. Rotational spectra of  $a^1\Delta_g$   $\text{O}_2$  isotopologues, *J. Chem. Phys.* **137**, 024305 (2012).
- [36] B. J. Drouin, S. Yu, B. M. Elliott, T. J. Crawford, and C. E. Miller, High resolution spectral analysis of oxygen. III. Laboratory investigation of the airglow bands, *J. Chem. Phys.* **139**, 144301 (2013).
- [37] D. Summers, B. Gregory, P. J. Stomski, Jr., A. Brighton, R. J. Wainscoat, P. L. Wizinowich, W. Gaessler, J. Sebag, C. Boyer, T. Vermeulen *et al.*, Implementation of a laser traffic control system supporting laser guide star adaptive optics on Mauna Kea, *Proc SPIE* **4839**, 440 (2003).
- [38] D. Summers, N. Apostolakos, R. Rutten, and G. Talbot, Second generation laser traffic control: Algorithm changes supporting Mauna Kea, La Palma, and future multi-telescope laser sites, *Proc SPIE* **6272**, 627244 (2006).
- [39] P. Amico, R. D. Campbell, and J. C. Christou, Laser operations at the 8–10 m class telescopes Gemini, Keck, and the VLT: Lessons learned, old and new challenges, *Proc SPIE* **7737**, 77370A (2010).
- [40] P. Amico, P. Santos, D. Summers, P. Duhoux, R. Arsenault, T. Bierwirth, H. Kuntschner, P.-Y. Madec, M. Prümm, and M. Rejkuba, The first component of the adaptive optics facility enters operations: The laser traffic control system on paranal, *The Messenger* **162**, 19 (2015).
- [41] E. Masciadri, J. Vernin, and P. Bougeault, 3D mapping of optical turbulence using an atmospheric numerical model. I. A useful tool for the ground-based astronomy, *Astron. Astrophys. Suppl. Ser.* **137**, 185 (1999).
- [42] C. d’Orgeville and G. J. Fetzer, Four generations of sodium guide star lasers for adaptive optics in astronomy and space situational awareness, *Proc SPIE* **9909**, 99090R (2016).
- [43] D. A. Leonard, Observation of Raman scattering from the atmosphere using a pulsed nitrogen ultraviolet laser, *Nature (London)* **216**, 142 (1967).
- [44] J. Cooney, Measurements on the Raman component of laser atmospheric backscatter, *Appl. Phys. Lett.* **12**, 40 (1968).
- [45] S. H. Melfi, J. Lawrence, and M. McCormick, Observation of Raman scattering by water vapor in the atmosphere, *Appl. Phys. Lett.* **15**, 295 (1969).
- [46] S. H. Melfi, Remote measurements of the atmosphere using Raman scattering, *Appl. Opt.* **11**, 1605 (1972).
- [47] J. Cooney, Measurement of atmospheric temperature profiles by Raman backscatter, *J. Appl. Meteorol.* **11**, 108 (1972).
- [48] P. Keckhut, M. L. Chanin, and A. Hauchecorne, Stratosphere temperature measurement using Raman lidar, *Appl. Opt.* **29**, 5182 (1990).
- [49] D. N. Whiteman, S. H. Melfi, and R. A. Ferrare, Raman lidar system for the measurement of water vapor and aerosols in the Earth’s atmosphere, *Appl. Opt.* **31**, 3068 (1992).
- [50] W. S. Heaps and J. Burris, Airborne Raman lidar, *Appl. Opt.* **35**, 7128 (1996).
- [51] A. Behrendt, T. Nakamura, M. Onishi, R. Baumgart, and T. Tsuda, Combined Raman lidar for the measurement of atmospheric temperature, water vapor, particle extinction coefficient, and particle backscatter coefficient, *Appl. Opt.* **41**, 7657 (2002).
- [52] U. Wandinger, Raman Lidar, in *Lidar: Range-Resolved Optical Remote Sensing of the Atmosphere*, Springer Series in Optical Sciences, edited by C. Weitkamp (Springer, New York, New York, NY, 2005), pp. 241–271.
- [53] J. D. Hunter, Matplotlib: A 2D graphics environment, *Comput. Sci. Eng.* **9**, 90 (2007).
- [54] T. P. Robitaille, E. J. Tollerud, P. Greenfield, M. Droettboom, E. Bray, T. Aldcroft, M. Davis, A. Ginsburg, A. M. Price-Whelan *et al.* (Astropy Collaboration), Astropy: A community Python package for astronomy, *Astron. Astrophys.* **558**, A33 (2013).
- [55] A. M. Price-Whelan, B. M. Sipőcz, H. M. Günther, P. L. Lim, S. M. Crawford, S. Conseil, D. L. Shupe, M. W. Craig, N. Dencheva *et al.* (Astropy Collaboration), The astropy project: Building an open-science project and status of the v2.0 core package, *Astron. J.* **156**, 123 (2018).
- [56] T. Robitaille and E. Bressert, APLpy: Astronomical plotting library in python, *Astrophysics Source Code Library*, ascl:1208.017 (2012).
- [57] F. P. A. Vogt, Fcmaker: Creating ESO-compliant finding charts for observing blocks on p2, *Astrophysics Source Code Library*, ascl:1806.027 (2018).
- [58] F. P. A. Vogt, Fcmaker: Automating the creation of ESO-compliant finding charts for observing blocks on p2, *Astron. Comput.* **25**, 81 (2018).
- [59] A package hosted at <https://astroquery.readthedocs.io>.
- [60] A. Ginsburg, M. Parikh, J. Woillez, A. Groener, S. Liedtke, B. Sipocz, T. Robitaille, C. Deil, B. Svoboda, E. Tollerud *et al.*, Astroquery: Access to online data resources, *Astrophysics Source Code Library*, ascl:1708.004 (2017).
- [61] B. M. Morris, E. Tollerud, B. Sipőcz, C. Deil, S. T. Douglas, J. Berlanga Medina, K. Vyhmeister, T. R. Smith, S. Littlefair, A. M. Price-Whelan *et al.*, Astroplan: An open source observation planning package in python, *Astron. J.* **155**, 128 (2018).

- [62] D. Foreman-Mackey, D. W. Hogg, D. Lang, and J. Goodman, Emcee: The MCMC hammer, *Publ. Astron. Soc. Pac.* **125**, 306 (2013).
- [63] F. Bonnarel, P. Fernique, O. Bienaymé, D. Egret, F. Genova, M. Louys, F. Ochsenbein, M. Wenger, and J. G. Bartlett, The ALADIN interactive sky atlas. A reference tool for identification of astronomical sources, *Astron. Astrophys. Suppl. Ser.* **143**, 33 (2000).
- [64] W. A. Joye and E. Mandel, New features of SAOImage DS9, *ASP Conf. Ser.* **295**, 489 (2003).